International Journal of Nanoelectronics and Materials
Volume 16, No. 2, April 2023 [407-420]

Structural, microstructural, dielectric and Ac-conductivity of $CaTi_{1-x}Fe_xO_3$ multiferroic materials synthesized by solid state method.

Najwa. Gouitaa [1,*] Abdelhalim.,Elbasset [1], Fatema Zahra. Ahjyaje [1], Taj-Dine. Lamcharfi [1], Farid. Abdi [1]

[1]Signals, Systems and Components Laboratory (LSSC), Electrical Engineering Department, University Sidi Mohamed Ben Abdellah USMBA, FST. Fez, Imouzzer Road B.P. 2202, Morocco.

Received 2 April 2022, Revised 18 July 2022, Accepted 11 August 2022

ABSTRACT

In this study, the structural, microstructural, dielectric and conductivity properties of Fe-doped $CaTiO_3$ (CT) ceramic were investigated. These ceramics were successfully synthesized using the conventional solid-state method. The X-ray diffraction and Rietveld refinement results showed that the ceramics at x=0.0, 0.1, 0.2 and 0.3 crystalized in the orthorhombic phase with the Pmmm space group. While for x=0.4, 0.5 and 0.6, the phase formation changes from orthorhombic to tetragonal phase with P4/mmm group space. The SEM results revealed a semi-spherical shape of grain for lower Fe content (≤0.4), while at x=0.5 and 0.6 an agglomeration phenomenon is observed and the observed density of the sample at x=0.5 is higher than the other ceramics. The dielectric properties were studied as function of frequency and temperature. The dielectric permittivity (ε'_r) decreases as function of frequency at lower frequency region and remain almost independent of frequency at high frequency region in the whole temperature range of R.T–520 °C. Each converges at high frequency (>10^5 Hz) for all the temperatures. The evolution of ε'_r as function of temperature for pure CT ceramic showed a stability at large range of temperature (from R.T to 250°C). For substituted ceramics, we obtained a phase transition which shifted to the lower temperature with the increase of Fe content. And the value of ε'_r, increases for Fe-doped CT ceramics and reaches a maximal value for x=0.5 which is 50 time bigger than the pure ceramic. The AC conductivity, σ_{AC}, is found to increase rapidly as a function of frequency, at low frequency region, and increases linearly at high frequency region, which confirms the hopping of electrons related to the conduction mechanism. The σ_{AC} evolution is found to follow the Jonscher's law and the s exponent decreased with the increasing temperature which is related to the correlated barrier height (CBH) model. And the σ_{AC} values increase with the increases of Fe content.

Keywords: conductivity, dielectric, phase transition, SEM, structural, X-ray diffraction.

1. Introduction

Perovskites are a large family of crystalline materials whose name derives from a natural mineral: calcium titanate ($CaTiO_3$). The use of $CaTiO_3$ can be found in several applications in the field of manufacturing electronic components, requiring high stability of electrical properties as a function of temperature. The $CaTiO_3$ material is active under UV light and presents an excellent photo-corrosion resistance with high thermal stability [1,2,3,4], which makes it a good candidate as a photocatalyst material. At low temperatures, it presents a ferroelectric property, and it has been used in electroluminescent devices and sensors. [1,5].

* Corresponding author: najwa.gouitaa@gmail.com

$CaTiO_3$ is a perovskite-like material of orthorhombic structure with *a* = 5.4398 Å, *b* = 7.6417 Å, and *c* = 5.3830 Å [6]. Its relative permittivity is about 183 at room temperature and 20 to 77 K [7]. In 1943, Naray-Szabo observed a distortion of the orthorhombic phase during heat treatments. Since then, the phase transitions of the perovskite $CaTiO_3$ have been fairly studied. Several works have reported a change from the orthorhombic structure (Pbnm) to the cubic structure $Pm\bar{3}m$ at high temperature. Vogt and Schmahl [8] found a phase transition from the orthorhombic Pbnm phase to the cubic phase Pm3m around 1290 °C; they did not observe any intermediate phase between these two phases. On the contrary, other researchers have reported the existence of one or more intermediate phases between these two phases. Thus, Guyot et. al [9] and Kennedy et. al [10] reported the presence of two intermediate phases between the Pbnm phase and the $Pm\bar{3}m$ phase. According to Guyot, the orthorhombic type (Cmcm) is stable between 1110 °C and 1250 °C while the tetragonal type is stable above 1250 °C. According to Kennedy, the orthorhombic phase (Cmcm) is stable between 1125 and 1220 ° C and the tetragonal structure (14 / mcm) is stable up to 1500 °C. On the other hand, Redfern [11] reported only one intermediate phase between the two phases Pbnm and Pm3m respectively. This was in fact the tetragonal phase (14 / mcm) which is found to be stable between 1250 and 1350 °C.

Generally, the structural and dielectric properties of $CaTiO_3$ are improved by appropriate substitutions of the Ca^{2+} or Ti^{4+} cations in the perovskite network with other types of cations [12, 13]. Recently, extensive studies have been carried out on the influence of different oxide additions on the properties of materials of the type $Ca_{1-x}M_xTi_{1-x}M'_xO_3$ (M = Y, Sr, Ba, Pb; M '= Co, Al, Fe, Cr). This class of materials has become very important and has found countless applications in manufacturing several electronic components [14,15]. The replacement of the Ti^{4+} cations by high valence ions creates additional negative charges, which are compensated by the positive charges created by the replacement of Ca^{2+} by lower valence ions which leads to the electric charge neutrality of the material.

The effects of different substitutions on the electrical properties of $CaTiO_3$ were reported [16]. The Fe-doped $CaTiO_3$ ceramic showed a potential application as semiconductor-based photocatalysis with the best photocatalytic activity, with degradation of almost 100 % MB (10 ppm) under UV–visible light for 180 min [17]. The results found showed that the substitution of Fe on the Ti site ensures the highest oxygen-ion and electronic conductivities. Dunyushkina et al. [18] measured the ionic and electronic conductivities of $CaTi_{1-x}Fe_xO_{3-\delta}$ (x =0-0.5) solid solutions and found that the ionic conductivity is maximal at x = 0.2 of Fe content, in concordance with other works [19, 20].

The conductivity is correlated with some structural changes as a function of Fe substitution. However, the electron and x-ray diffraction (XRD) studies [21] show that, in $Ca_2T_{2-2-x}Fe_{2x}O_{6-x}$ solid solutions with $0 < x \leq 0.4$, oxygen vacancies are arranged at random, so that the materials retain pseudocubic symmetry; in the composition range $0.55 \leq x < 1$, the vacancies undergo ordering in the (0k0) plane. McCammon et al. [22] reported that the x = 0.38 material had a well-defined domain structure with domain sizes in the range 5–10 nm. They explained these results by the ordering of oxygen vacancies. In this study we studied the structural change of Fe doped $CaTiO_3$ ceramics as a function of Fe substitution for x=0.0 to 0.6 and correlated it with dielectric and conductivity properties.

So, in this work, we synthesized the Fe^{3+} doped $CaTiO_3$ ceramic using the solid-state method for x=0.0 to 0.6 of Fe content. We correlate the structural, dielectric and conductivity properties of these ceramics depending on Fe content. We have compared all the obtained results with the other reported works.

2. EXPERIMENTAL AND METHOD

The Fe-doped $CaTiO_3$ ceramics with the general formula: $CaTi_{1-x}Fe_xO_{3-\delta}$ for x=0.0 to 0.6 of Fe content, were elaborated by the conventionnel solid-state method. The starting powders are constituted by $CaTiO_3$, TiO_2 and Fe_2O_3 (with high purity higher than 99%, Sigma Aldrich). These precursors were mixed with acetone and stirred for 4 h, and then dried for 24 h at a temperature of 80 ° C in the oven. After drying, the powder obtained was ground for approximately 45 min, then calcined in the oven at a temperature of 1300 °C for 4 h, and then reground for 30 min.

We used the X-ray diffraction (XRD) to determine the structure and crystallographic orientations of materials. This technique studies the X-ray diffraction of a sample after the interaction of these rays with the atoms of the material. The measuring equipment used is Siemens X'Pert diffractometer. The monochromatic X–ray radiation is produced by a copper anticathode Kα line. The filter is a nickel pellet (Ni) for filtering the doublet Kα1, Kα2 characterized by an average wavelength λkα = 1.5406 A°. The continuous acceleration voltage used is 40 kV and the heating current is 30 mA. The results obtained were fitted using Rietveld refinement with FullProf software.

Then, we prepared the pellet from the calcined powders. So, the powders obtained are mixed with 2% APV (polyvinyl alcohol) already prepared. The mixture is dried in an oven at 80 °C, and then grinded. The fine powder is pressed using uniaxial pressure of 6 tons to form a pellet. The pellets obtained are sintered at 1200 °C/6 h with an ascent rate equal to 2 °C./min. The particle size and morphology of the pellets were observed by a scanning electron microscope (SEM) with JSM-IT500HR instrument. Both sides of the pellets are metalized using the silver lacquer, a metal layer to study the electrical and dielectric properties measurements. The dielectric properties were studied with Agilent E4980A by varying the temperature from room temperature (R.T) to 550 °C and frequency (from 20Hz to 2MHz).

3. RESULTS AND DISCUSSION

3.1 X-ray diffraction results

To choose the adequate calcination temperature of the $CaTi_{1-x}Fe_xO_{3-\delta}$ (CTF) powders, we study the phase stability as a function of the calcination temperature for the sample at x = 0.5 ($CT_{0.5}F_{0.5}$), at different temperatures 1100 °C, 1200 °C and 1300 °C for 4 hours. Figure 1 shows the XRD results of these compounds. We can notice, at 1100 °C and 1200 °C, a presence of peaks which were ascribed to the perovskite-type structure of tetragonal symmetry (marked with stars) with the highest intensity is at 2Θ= 33.5°, and the presence of secondary phases (marked with red points). While at 1300°C, the impurities disappear, and the material remains stable and crystallizes in a tetragonal phase. Hence, we have chosen 1300 °C as the calcination temperature of all the $CaTi_{1-x}Fe_xO_{3-\delta}$ ceramics.

The XRD results from $CaTi_{1-x}Fe_xO_{3-\delta}$ (CTF) ceramics, for x=0.0 to 0.6 of Fe content, are shown in Figure 2 and reveal that all the powders crystallize in a pure phase without the presence of secondary phases expect the sample at x=0.6 of Fe content. For pure CT (x=0.0), we can observe the formation of peaks characteristic of the orthorhombic phase, while at x=0.6 the tetragonal peaks are found. To study the phase change between these percentages (x = 0.1 to 0.6) or if we have the coexistence of two phases, we used the Rietveld method.

The Rietveld refinement results of CTF ceramics, for x=0.0 to 0.6 of Fe content, are shown in Figure 3. For pure CT (x=0.0), Figure 3(a) and Table 1, show that the powder crystallizes in the pure orthorhombic phase with the space group of Pmmm without the presence of any secondary

phase. These results are in contradiction with those reported by Guyot et. al [9] and Kennedy et. al [10] in which the tetragonal structure (14 / mcm) is stable from a temperature above 1250 °C. With the increase in Fe content from 0.0 to 0.3, we notice no change in the structure and space group of CTF ceramics. While for $x \geqslant 0.4$, the structure of CTF changes from orthorhombic to tetragonal phase with P4/mmm space group and we observe an appearance of secondary phases for x=0.6 (indicated by stars) which is probably due to the Ti-site saturation. So, there was no phase mixture in these ceramics like for the Fe-doped $BaTiO_3$ ceramics [23] in which we have found a coexistence of two phases for x=0.10 to 0.30 of Fe contents. These results are not the same as those reported by L. A. Dunyushkina et. al [18] for the same ceramics, in which they found that the Fe-doped $CaTiO_3$ has a cubic symmetry.

The effect of Fe^{3+} substitution on the lattice parameters and the unit cell volume values is shown in Table 1. The change in these parameters depending on the doping rate is related to the ionic radii of Fe^{3+} (0.76 Å), which may substitute Ca^{2+} (0.06 Å), Ti^{2+} (0.80 Å) or Ti^{4+} (0.64 Å), or it is due to the presence of vacancies. However, at a low Fe rate (x =0.1), Fe^{3+} may substitute Ti^{4+} or there is a creation of vacancies which causes an increase in the lattice constants and, so, an expansion of the unit cell. While at high Fe concentration (x=0.2 and 0.3), Fe^{3+} may replace Ca^{2+} and / or Ti^{4+}, which causes a decrease of the lattice constants that cause contraction in the unit cell.

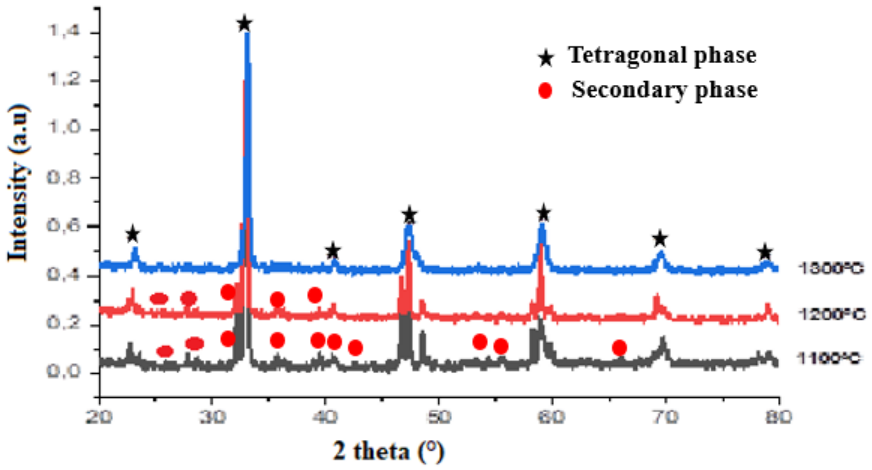

Figure 1. X-ray diffraction of ceramic $CT_{0.5}F_{0.5}$ calcined at different temperature.

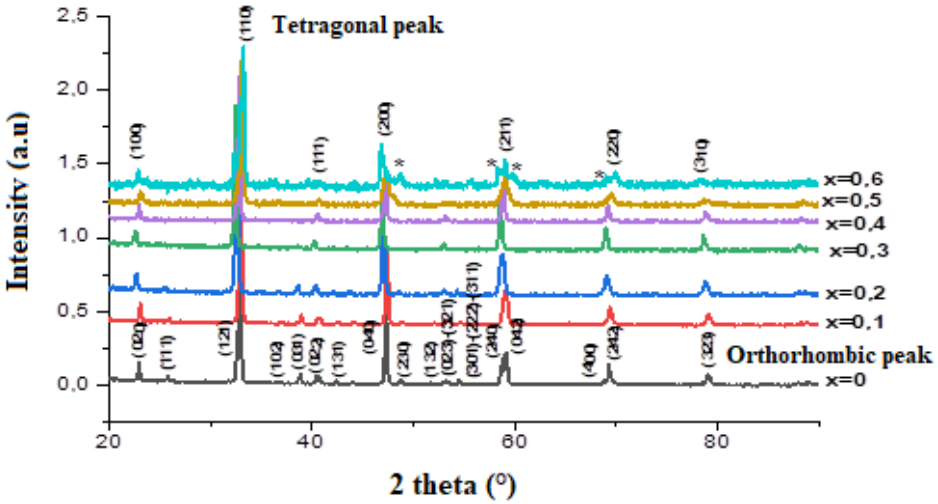

Figure 2. X-ray diffraction of ceramic CTF for x=0.0 to 0.6 calcined at 1300 °C/4h.

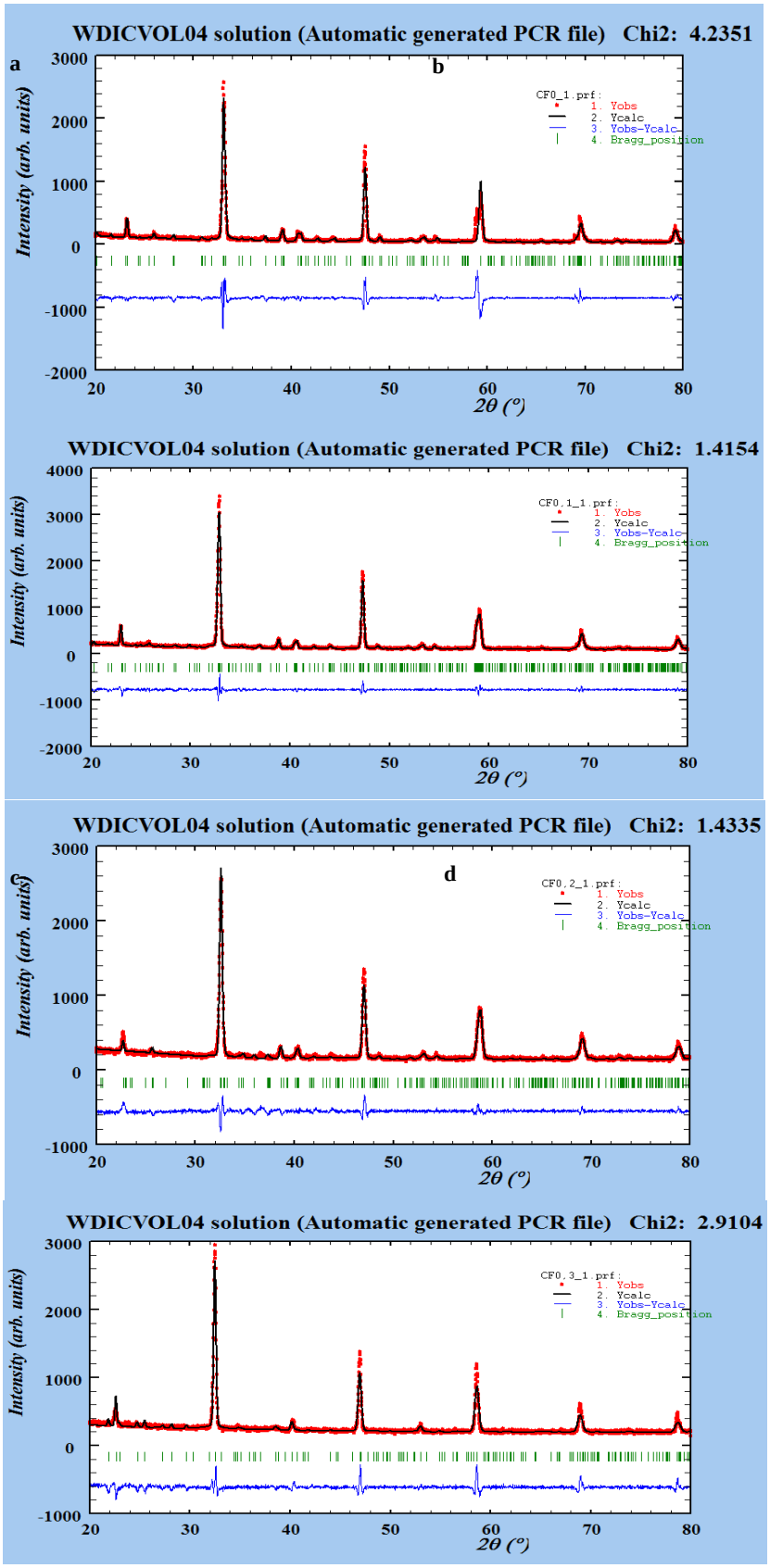
WDICVOL04 solution (Automatic generated PCR file) Chi2: 4.2351
a
b
CF0_1.prf:
1. Yobs
2. Ycalc
3. Yobs-Ycalc
4. Bragg_position
Intensity (arb. units)
2θ (°)
WDICVOL04 solution (Automatic generated PCR file) Chi2: 1.4154
CF0_1_1.prf:
1. Yobs
2. Ycalc
3. Yobs-Ycalc
4. Bragg_position
Intensity (arb. units)
2θ (°)
WDICVOL04 solution (Automatic generated PCR file) Chi2: 1.4335
c
d
CF0_2_1.prf:
1. Yobs
2. Ycalc
3. Yobs-Ycalc
4. Bragg_position
Intensity (arb. units)
2θ (°)
WDICVOL04 solution (Automatic generated PCR file) Chi2: 2.9104
CF0_3_1.prf:
1. Yobs
2. Ycalc
3. Yobs-Ycalc
4. Bragg_position
Intensity (arb. units)
2θ (°)

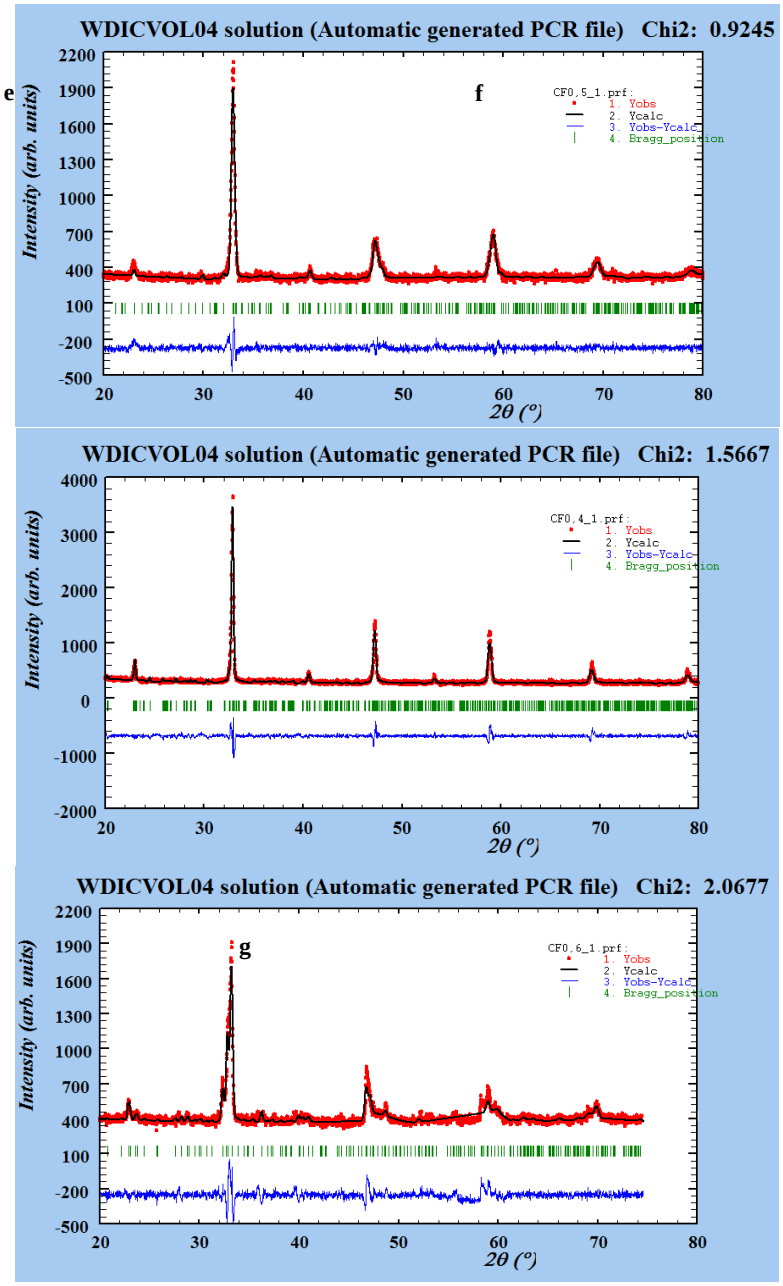

Figure 3. Rietveld refinement results of CTF ceramic for (a) x= 0,0; (b) x=0,1; (c) x=0,2; (d) x=0,3; (e) x=0,4; (f) x=0,5; (g) x=0,6.

Table 1. Unit cell parameters of CTF for x = 0.0 to 0.6 of Fe content.

Fe content	x=0	x=0,1	x=0,2	x=0,3	x=0,4	x=0,5	x=0,6
Unit cell parameter	**a**=11.479Å **b**= 7.691Å **c**= 4.402Å **V**=388.72Å^3	**a**=21.85Å **b**= 8.178 Å **c**= 3.853 Å **V**=688.7 Å^3	**a**=8.682 Å **b**=8.612 Å **c**=7.823 Å **V**=584.915Å^3	**a**=8.116 Å **b**=7.733 Å **c**=5.504 Å **V**=345.478Å^3	**a**= **b** =7.672 Å **c**=22.334 Å **V**=1314.41 Å^3	**a**= **b** =8.12Å **c**=24.46 Å **V**=1612.6Å^3	**a**= **b** =15.4 Å **c**=5.926 Å **V**=1406.4 Å^3
Space group	Pmmm	Pmmm	Pmmm	Pmmm	P4/mmm	P4/mmm	P4/mmm

3.2 SEM results

The Figure 4 shows the SEM micrographs of pure $CaTiO_3$ and Fe-doped $CaTiO_3$ samples sintered at 1200 °C for 6h. As it is shown, the size and morphology of the samples change depending on Fe content. However, the sample particles have semi-spheric shapes for x=0.0 and 0.1, while those at x=0.2 to 0.4 show a quadratic shape. According to Gheffar KhKara et. al [24], the spherical shape is attributed to the CT material, and this is why it is observed in samples with low Fe rate. For x=0.5, we can't observe a grain shape due to the high grain size. This sample exhibits a high density which decreases for x=0.6 sample because the latter contains a significant number of pores. In addition, the substituted ceramic's particles, at 0.6 of Fe content show a significant agglomeration phenomenon, which is related to the highly reactive nature of Fe ions [25,26]. This agglomeration phenomenon was also observed by He Yang et. al for Fe-doped $CaTiO_3$ ceramics as a function of calcination temperature [26] and Fe substitution content [28]. We can also notice a clear decrease in grain size for x= 0.1, 0.2 and 0.3 of Fe content which is equal to 3.32, 2.675, and 1.89 µm respectively**,** and above 0.3 of Fe rate, the grain size increases significantly. The same grain size evolution was reported in our previous work for Fe-doped $BaTiO_3$ ceramics (for x=0.0 to 0.6) [29]. The decrease in grain size is caused by the creation of oxygen vacancies which generate a lattice distortion, found in XRD results. However, Ohno et. al. [30]. reported a crystal growth inhibition for Fe-doped $CaTiO_3$ related to the oxygen vacancies that create a pining site and cause a decrease in ion mobility.

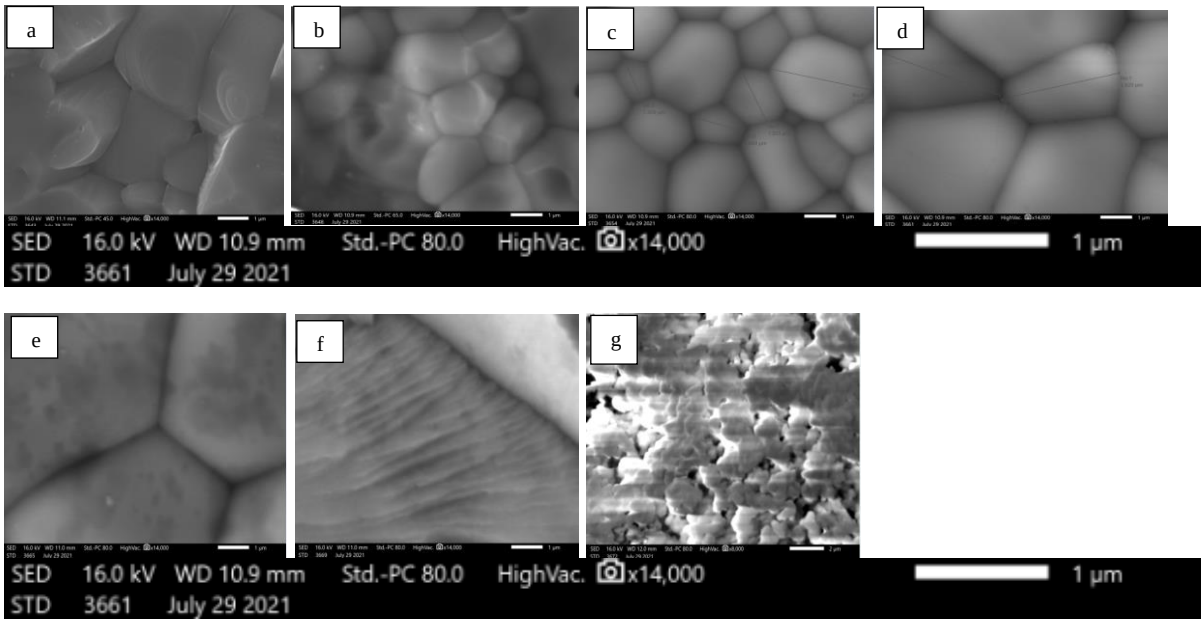

Figure 4. SEM Micrographs of CTF pellets for x= (a) 0.0; (b) 0,1; (c) 0.2; (d) 0.3; (e) 0.4; (f) 0.5 and (g) 0.6.

3.3 Dielectric properties

The frequency dependence dielectric permittivity for CTF ceramics (at x=0.0 to 0.6) is shown in Figure 5. All the ceramics follow the same behavior named classical ferroelectrics behavior. However, the dielectric permittivity is high at low frequency region and decreases rapidly with the increase of frequency; after that, it remains constant at high frequency region. This evolution of dielectric permittivity as a function of frequency is related to the interfacial polarization known by Maxwell–Wagner. The high value of the dielectric permittivity at low frequency, is due to the presence of polarization of the space charges at the grain boundaries, generating a potential barrier which leads to an increase in the values of the real part of the permittivity [31]. To explain the decrease in the real part of the permittivity at high frequencies, it is assumed that the dielectric structure is composed of grains of low resistance separated by fine and weakly conductive grain boundaries. With the application of an electric field, interfacial polarization is created due to the localized accumulation of charges [32].

The effects of Fe^{3+} doping ions on the temperature dependence of the dielectric properties of the CT ceramics are shown in Figure 5. Notably, the Fe^{3+} doping ions can enhance the temperature stability of ε'_r. However, the dielectric permittivity of CT ceramic (Figure 6(a)) does not change with temperature variation at a large range of temperature from R.T to 250 °C, after that, it increases rapidly. The same behavior is observed for x=0.1 and 0.2 of Fe contents (figure.6. b and c). While for x ≥0.3, the dielectric permittivity is no longer stable as a function of temperature, it increases and reaches a maximum showing a phase transition T_m. This phase transition presents a diffuse phenomenon which becomes more important with the increase of frequency, and it shifts to the lower temperature with the increase in Fe content (Table.2). The same behavior is reported in our previous work for Fe doped $BaTiO_3$ ceramic [23].

From Table 2, we can also notice that the dielectric permittivity for substituted ceramics (from x=0.1 to 0.5) is higher than the pure CT, and it is maximal for x=0.5, then it decreases for x=0.6 of Fe content. However, the lower value of ε'_r at x=0.6 of Fe content is due to the appearance of pores in this sample. While ε'_r, for the sample at x=0.5, has a colossal value which is about 50 times bigger than the pure CT ceramic, which is probably due to the high density of this pellet found in SEM results. So, the dielectric properties of CT ceramic are improved by Fe substitution. This dielectric permittivity evolution differs from the results of BT substituted with Fe [22]. In which the Fe substitution decreases the ε'_r value of $BaTiO_3$ ceramic.

Regarding the ε'_r value of Fe-doped $BaTiO_3$ sample prepared by solid state method [22] and this of Fe doped-$CaTiO_3$ in this study, these materials can be used for passive components into various types of dielectrics regarding their functionality. Based on these values, the Fe-$BaTiO_3$ have a lower ε'_r value at high temperature, which can be useful at Class 1 of dielectric capacitors named C0G, while Fe-$CaTiO_3$ with higher ε'_r value can be applicated for Class 2 of dielectric capacitors named X5R. These two dielectrics codes of Class 1 and 2 have been classified by the Electronic Industries Alliance (EIA) [33].

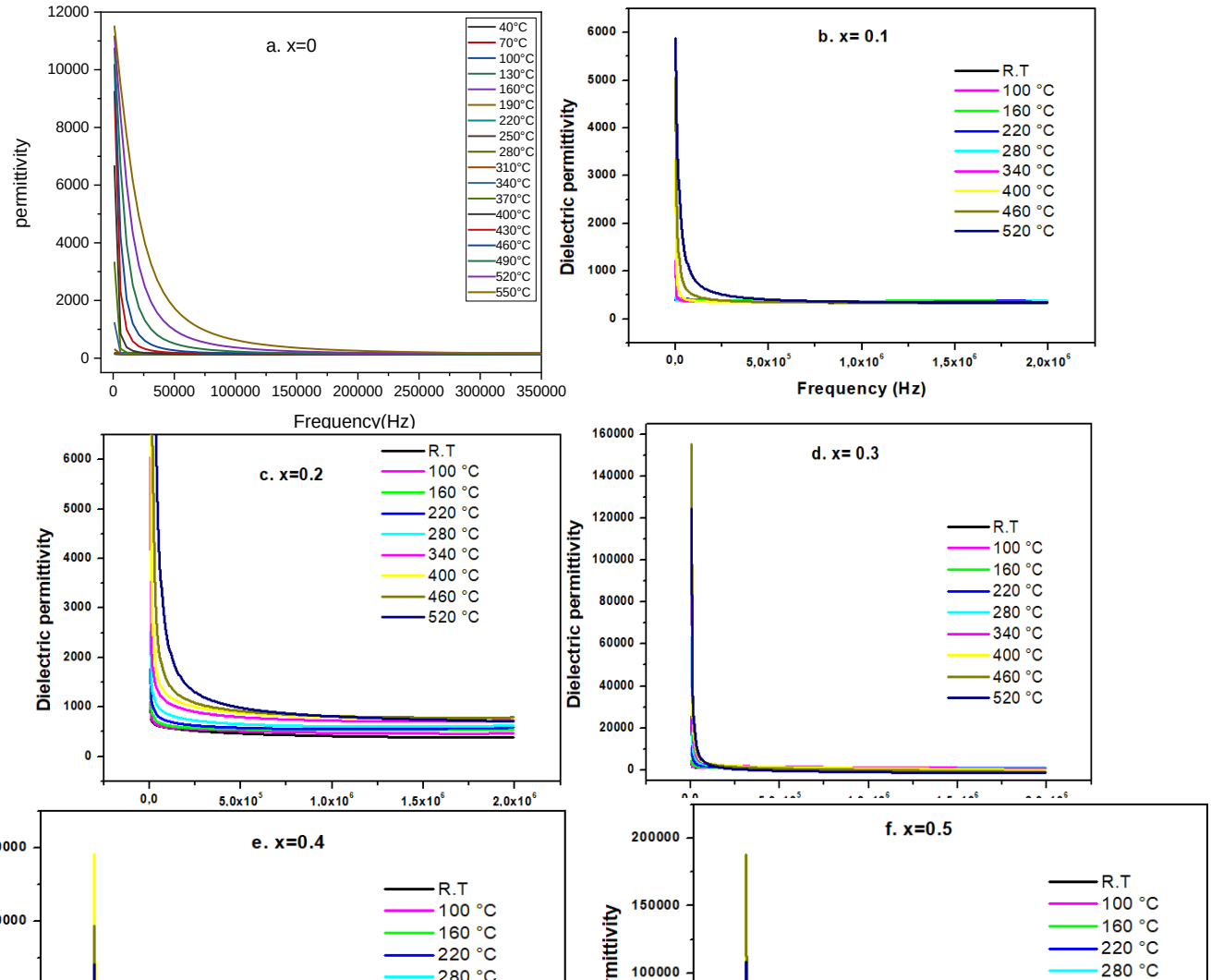

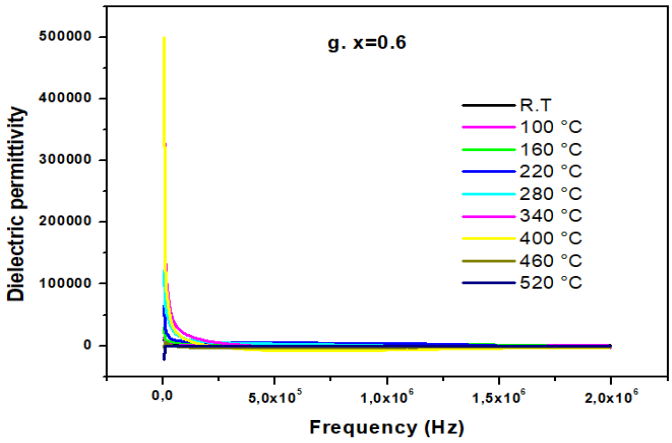

Figure 5. Frequency dependence of dielectric permittivity of CTF ceramics for x= (a) 0.0; (b) 0.1; (c) 0.2; (d) 0.3; (e) 0.4; (f) 0.5 and (g) 0.6.

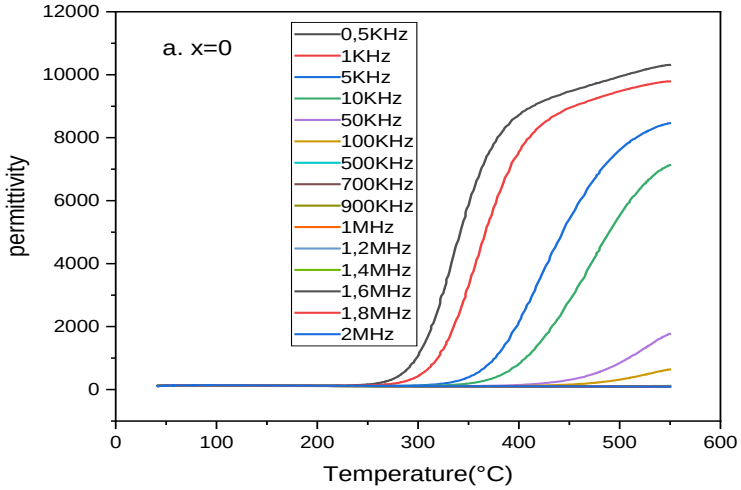

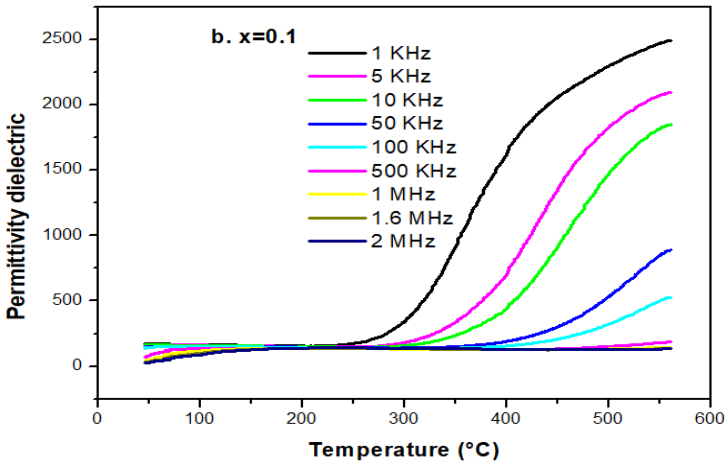

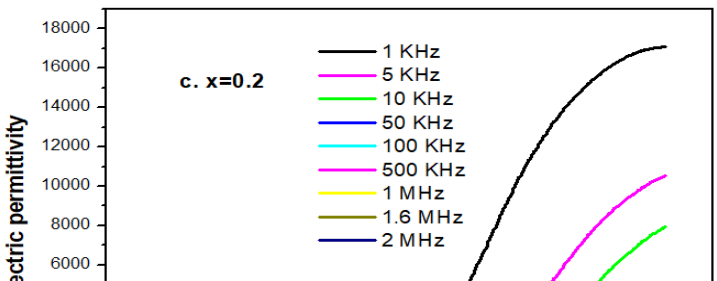

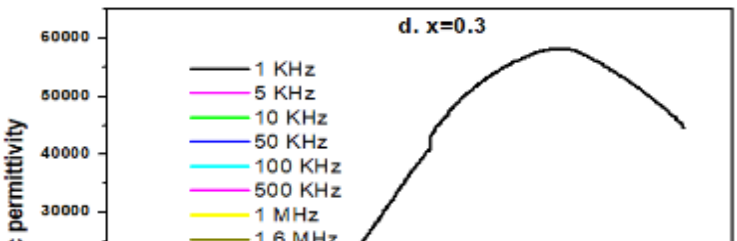

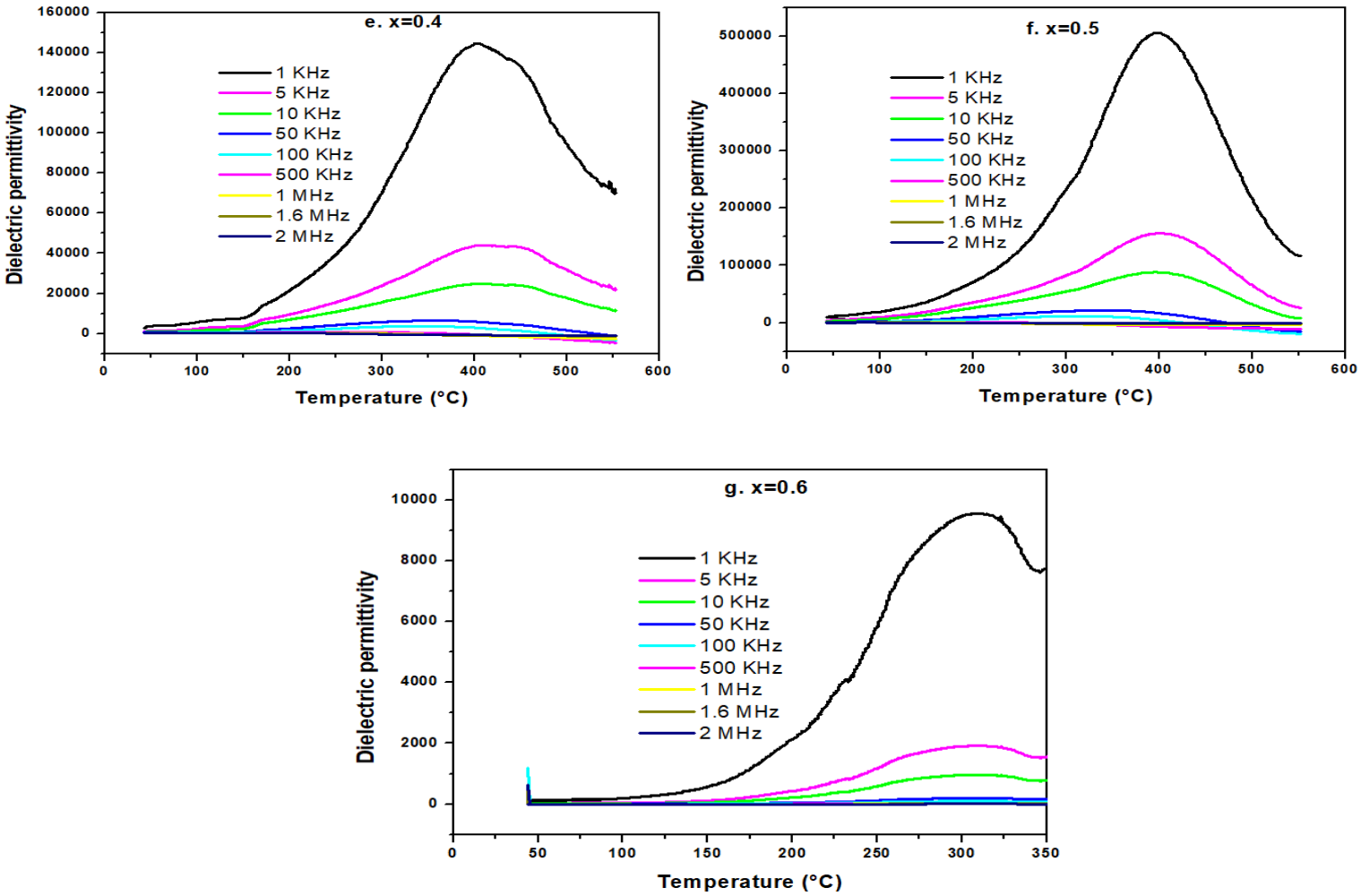

Figure 6. Temperature dependence of dielectric permittivity of CTF ceramics for x= (a) 0.0; (b) 0.1; (c) 0.2; (d) 0.3; (e) 0.4; (f) 0.5 and (g) 0.6.

Table 2. Phase transition, Tm and the dielectric permittivity, ε'_r of CTF ceramics for different Fe content at the frequency of 1 kHz

FT rate	**T_m(°C)**	**$\varepsilon'r$**
0	$T_m \geq 550$	$\varepsilon'r \geq 10279$
0.1	$T_m \geq 550$	$\varepsilon'r \geq 2493$
0.2	$T_m \geq 550$	17 091

0.3	405	143 774
0.4	414	57 811
0.5	398	**505 961**
0.6	302	9 503

3.4 Ac conductivity study

Figure 7(a) shows the evolution of AC conductivity as a function of frequency in the frequency range of 20 Hz–2 MHz at different temperatures in the range of R.T to 520 °C for CTF ceramic at x=0.1. It can be seen that σ_{AC} increases rapidly, at low frequency region, as the frequency is increased because the admittance of the capacitor is numerically larger than the admittance of the resistor as the frequency increases. Above 10^5 Hz of frequency (high frequency region), the σ_{AC} increases linearly with increasing frequency. This linear increase of σ_{AC} with increasing frequency is probably related to the hopping of electrons, atoms, and motion between sites [34].

The dispersion in conductivity in these ceramics can be described by Jonscher's law [35] according to the relation (1):

$$\sigma_\omega = \sigma_{dc} + A\,\omega^s. \quad (1)$$

Where σ_ω is the AC conductivity, $\omega = 2\pi f$ is the angular pulsation, and s is the power law exponent, $0 < s < 1$. And A is a constant which is dependent poorly on temperature.

The values of exponent s at different temperatures of CTF (for x=0.1) ceramic are tabulated in Table 3. These values of s are determined from the slope of the linear σ_{AC} versus frequency curve. The s values are between 0.40 and 0.99 and s decreases with increasing temperature. This behavior of s with temperature variation shows a conduction mechanism in these ceramics which is related to the barrier jump model correlated (CBH), according to which the transport of charges occurs between localized states related to a jump of the potential barriers. We have found the same variation of s for Fe-substituted $BaTiO_3$ ceramics [23].

The σ_{AC} exhibits similar curve shapes with increasing frequency and at different temperature values for other doped samples. The Figure 6(b) shows σ_{AC} as a function of temperature for pure and substituted CTF ceramics (for x=0.0 to 0.6) at R.T. As expected, the σ_{AC} value increases with the increase of Fe content for all the substituted ceramics, which makes its capacitive applications difficult. The same effect of Fe substitution on conductivity values is reported in our previous work [23], and was also reported by S.J.T. Vasconcelos et. al [36] for $CaTiO_3$-$LaFeO_3$ ceramics. But this result contradicts with those found by L.A Dunyushkina, which reported that the conductivity is maximal at 0.2 of Fe content then it decreases.

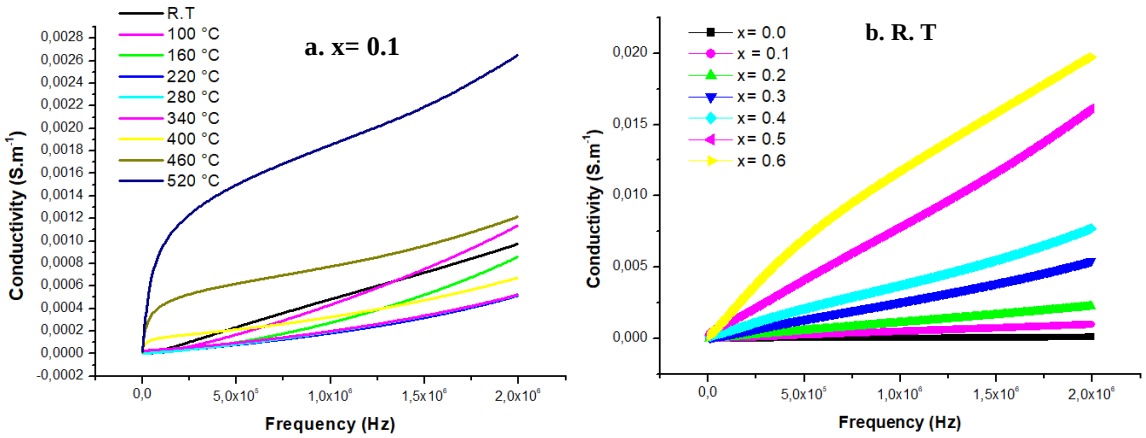

Figure 7. The Frequency dependence of conductivity of (1-x) CT-x FT composites (a) for x= 0.1 at different temperature; (b) for x= 0.0 to 0,6 at R.T.

Table 3. The s values of CTF for x = 0.1 of Fe content at different temperatures.

Temperature (°C)	s
R. T	0.99
100	0.97
160	0.93
220	0.90
280	0.83
340	0.75
400	0.47
460	0.36
520	0.40

Conclusion

The $CaTi_{1-x}Fe_xO_{3-\delta}$ (CTF) powders were successfully synthesized by using the conventional solid-state method. The X-ray diffraction results confirm the orthorhombic phase formation for x≤0.3, while above this rate, the structure changes from orthorhombic to tetragonal phase. The microstructure of the sintered samples showed a decrease in grain size for x≤0.3, then it increased for x=0.4 and 0.5. In addition, the density of the sample at x=0.5 is higher. The dielectric properties of CTF ceramics revealed a phase transition for substituted ceramics which shifted to the lower temperature with the increase in Fe doping. And ε'_r were improved for substituted ceramics, especially for x=0.5, which is 50 times bigger than the pure CT ceramic. This highest permittivity in this study is related to the highest relative density found for this sample. For this, the CTF (at x=0.50) can be used in ceramic capacitors and high energy density storage applications. On the other hand, the AC conductivity, σ_{AC}, is found to follow Jonscher's law. The frequency exponent s decreases with increasing temperature, so the results of the σ_{AC} are related to the correlated barrier height (CBH) modeland the AC conductivity value increases with the increase of Fe content.

References

[1] Pereira, S.C., Figueiredo, A.T., Barrado, C.M., Stoppa, M.H., Dwivedi, Y., Li, M.S., Longo, E., J. Braz. Chem. Soc. 26 (2015) 2339-2345.
[2] Han, C., Liu, J., Yang, W., Wu, Q., Yang, H., Xue, X., J. Photochem. Photobiol. A-Chem. 322 (2016) 1-9.
[3] Grabowska, E., A review, Appl. Catal. B-Environ. 186 (2016) 97-126.
[4] Han, C., Liu, J., Yang, W., Wu, Q., Yang, H., Xue X., J. Sol-Gel Sci. Technol. 322 (2016).
[5] Cheng, Z., Lin, J. , Crystengcomm. 12 (2010) 2646-2662.
[6] Wong, Y. J., Hassan, J., Hashim, M., Journal of Alloys and Compounds. 571, (2013) 138-144.
[7] Zhang, L., Wang, X., Liu, H., Yao, X., J. Am. Ceram. Soc., 93 (2010) 1049–1055.
[8] Vogt, T., Schmahl, W., Euro. phys. Lett, 24, (4) (1993), 281-285.
[9] Guyot, F., Richet, P., Courtial, Ph., and Gillet, Ph., Phys. Chem. Minerals, 20 (1993) 141-146.
[10] Kennedy, B.J., Howard, C.J., Chakoumakos, B.C., J. Phys. Cond. Matter, 11 (1999) 1479-1488.
[11] Redfern, S.A.T., J. Phys. Cond. Matter. 8 (1996) 8267-8275.

[12] Kipkoech, E.R., Azough, F., Freer, R., Leach, C., Thomposon, S.P., Tang, C.C., J. Eur. Ceram. Soc., 23 (2003) 2677-2682.
[13] Yoon, M. S., Ur, S. C., Ceramics International, 34 (2008) 1941-1948.
[14] Chen, G. H., Chen, J. S., Kang, X. L., Yang, T., Luo, Y., Yuan, C. L., Zhou, C. R., Journal of Materials Science: Materials in Electronics volume 28 (2017) 6301–6307.
[15] Zou, J., Zhang, T., He, X., Materials Letters, 248 (2019) 173-176.
[16] Dunyushkina, L., Gorbunov, V. A., Inorganic Materials 37(11): (2001) 1165-1169.
[17] Yang, H., Han, C., Xue, X., Journal of Environmental Sciences, 26 (2014) 1489-1495.
[18] Dunyushkina, L.A., Demin, A.K., Zhuravlev, B.V., Solid State Ionics, 116, (1999) 85–88.
[19] Sutija, D.P., Norby, T., Osborg, P.A., and Kofstad, P., Electrochem. Soc. Proc., vol. 93 (1993) 552–557.
[20] Gorelov, V.P. and Balakireva, V.B., Elektrokhimiya, 33 (1997) 1450–1454.
[21] Grenier, J.C., Schiffmacher, G., Caro, P., J. Solid State Chem., 20 (1977) 365–379.
[22] McCammon, C.A., Becerro, A.I., Langenhorst, F., et al., Phys.: Condens. Matter., 12 (2000) 2969–2984.
[23] Gouitaa, N., Lamcharfi, T., Bouayad, MF., Abdi, F., Echatoui, N.S., and Hadi, N., Asian Journal of Chemistry, 29 (2017) 2143-2148.
[24] Kara, G. K., Moshari, M., Rabbani, M., Rahimi, R., Materials Chemistry and cs, 259, (2021) 124062
[25] Keswani, B. C., Devan, R. S., Kambale, R. C., James, A. R., Manandhar, S., Kolekar, Y. D., Ramana, C. V., J. Alloys Compd., 712 (2017) 320-333.
[26] Medeiros, P. N., Araújo, V. D., Marques, A. P. A., Tranquilin, R. L., Paskocimas, C. A., Bomio, M. R. D., Varela, J. A., Longo, E., Motta, F. V., J. Adv. Ceram., 4 (2015) 65-70.
[27] Yang, H., Han, C., Xue, X., Journal of Environmental Sciences, 26 (2014) 1489-1495.
[28] Han, C., Yang, H., Xue, X.,Trans. Nonferrous Met. Soc. China 24 (2014) 3215−3220.
[29] Gouitaa, N., Lamcharfi, T., Bouayad, M., Abdi, F., Hadi, N., Journal of Materials Science: Materials in Electronics (2018).
[30] Ohno, T., Ochibe, S., Wachi, H., Hirai, S., Arai, T., Sakamoto, N., Suzuki, H., and Matsuda, T., Adv. Pow. Tech., 29, (2018) 584-589.
[31] Abdullah Dar, M., Majid, K., Mujasam Batoo, K., Kotnala, R. K., J. Alloys Compd. 632 (2015) 307–320.
[32] Rahmouni, H., Smari, M., Cherif, B., Dhahri, E., Khirouni, K., Dalton Trans. 44 (2015) 10457–10466,
[33] Mikkenie, R., Advances in Physics, 31 (1982) 553-637.
[34] Jonscher, A.K., Nature 267 (1977) 673–679.
[35] Vasconcelos, S.J.T., Silva, M.A.S., de Oliveira, R.G.M., Bezerra Junior, M.H., de Andrade, H. D., Queiroz Junior, I.S., Singh, C., Sombra, A.S.B., Materials Chemistry and Physics 257 (2021) 123239.